

# Hydrodynamic approach to electronic transport in graphene

B.N. Narozhny,<sup>1,2</sup> I.V. Gornyi,<sup>1,3,4</sup> A.D. Mirlin,<sup>1,3,5</sup> and J. Schmalian<sup>1,6</sup>

<sup>1</sup>*Institute for Theoretical Condensed Matter Physics,  
Karlsruhe Institute of Technology, 76128 Karlsruhe, Germany*

<sup>2</sup>*National Research Nuclear University MEPhI (Moscow Engineering  
Physics Institute), Kashirskoe shosse 31, 115409 Moscow, Russia*

<sup>3</sup>*Institute of Nanotechnology, Karlsruhe Institute of Technology, 76021 Karlsruhe, Germany*

<sup>4</sup>*Ioffe Physical Technical Institute, 194021 St. Petersburg, Russia*

<sup>5</sup>*Petersburg Nuclear Physics Institute, 188300 St. Petersburg, Russia*

<sup>6</sup>*Institute for Solid State Physics, Karlsruhe Institute of Technology, 76021 Karlsruhe, Germany*

The last few years have seen an explosion of interest in hydrodynamic effects in interacting electron systems in ultra-pure materials. In this paper we briefly review the recent advances, both theoretical and experimental, in the hydrodynamic approach to electronic transport in graphene, focusing on viscous phenomena, Coulomb drag, non-local transport measurements, and possibilities for observing nonlinear effects.

Hydrodynamics describes a great variety of phenomena around (and inside) us, including, e.g., the flow of water in rivers, seas, and oceans, atmospheric phenomena, aircraft motion, the flow of petroleum in pipelines, or the blood flow through blood vessels in humans and animals. It has been realized a long time ago that the flow of electrons in a conductor should, under certain circumstances, also obey the laws of hydrodynamics. In particular, Gurzhi<sup>1,2</sup> predicted that electrons can exhibit a Poiseuille-type flow<sup>3,4</sup> analogous to that of liquids in pipes. This should result in an initial power-law decrease of resistivity with the transverse cross-section of a sample and temperature, leading to a pronounced minimum. It has turned out, however, that an experimental realization of such a regime in a metal or a semiconductor is a highly non-trivial task. Three decades have passed before de Jong and Molenkamp<sup>5</sup> observed the Gurzhi effect, and even in that work the magnitude of the effect did not exceed 20%.

Why is it so difficult to implement electron hydrodynamics in a laboratory experiment? In contrast to molecules of a conventional liquid, electrons move in the environment formed by the crystal lattice. Therefore, the electrons experience not only collisions among themselves, but also scatter off thermally excited lattice vibrations – phonons – as well as various lattice imperfections (impurities). The hydrodynamic regime is realized when the frequency of electron-electron collisions is much larger than the rates of both, electron-phonon and electron-impurity scattering. These two requirements limit the temperature window for the hydrodynamic flow both from above and from below, and may even be in a conflict with each other. In a typical solid, the elastic impurity scattering dominates electronic transport at low temperatures, whereas at high temperatures the leading mechanism is the electron-phonon scattering. Thus, the requirement of the electron-electron scattering being the fastest process – which is the key condition for the hydrodynamics – may only be satisfied, if at all, in an intermediate temperature range. It turns out that this regime is not well developed in conventional conductors, with the

possible exception of the ultrahigh-mobility *GaAs* quantum wells<sup>6–8</sup> exhibiting negative magnetoresistance<sup>9</sup> and ultra-pure palladium cobaltate<sup>10</sup>.

The experimental discovery of graphene<sup>11</sup> has given a new boost to the research in the field of quantum transport. In particular, it has been realized that, among other remarkable properties, graphene is an excellent material for the realization of hydrodynamic flow of electrons<sup>12–14</sup>. The reasons for this are as follows. First, electron-phonon scattering in graphene on suitable substrates is rather weak, which manifests itself in unprecedentedly high carrier mobilities at elevated temperatures. Second, the progress in fabrication allows to produce graphene samples of outstanding quality (i.e. with a very low concentration of impurity atoms or lattice defects)<sup>15,16</sup>. An additional twist to the story is provided by the “quasi-relativistic” excitation spectrum of graphene near charge neutrality – that of massless 2D Dirac fermions. A fluid emerging in this situation is formed by two species of carriers with opposite charges – electrons and holes<sup>17</sup>.

The emergent two-fluid hydrodynamics in graphene is neither Galilean-, nor Lorentz-invariant<sup>18–23</sup>. The former feature is a consequence of the linearity of the excitation spectrum yielding the strong dependence of the transport scattering time in graphene on electron-electron interaction<sup>24</sup>. The latter appears due to the classical (and moreover, three-dimensional) nature of the Coulomb interaction between charged quasiparticles in graphene. As a result, rather than assuming the standard approach<sup>22,23,25</sup> the hydrodynamic equations have to be derived from the microscopic theory<sup>18,19,26–28</sup>.

Microscopically, the motion of the charge carriers may be described using the methods of the kinetic theory<sup>25</sup>. At the simplest level, transport properties of conventional metals and semiconductors are determined by means of a perturbative solution of the kinetic equation under the assumption of a weak external bias (i.e. the electric field or temperature gradient). Final results are typically expressed in terms of the linear relations between the macroscopic currents and the external fields, e.g. Ohm’s

law. The proportionality coefficients, such as the electrical resistivity, are determined by the rates of momentum-nonconserving scattering processes – disorder scattering at low temperatures and electron-phonon scattering at high temperatures. Inelastic scattering processes responsible for the equilibration of the system are assumed to be much faster than any transport-related time scale. In contrast, the hydrodynamic behavior appears when the dominant scattering process in the system is due to electron-electron interaction. In conventional systems, this may happen either in pure Fermi liquids<sup>29</sup>, clean samples in constricted geometries<sup>1</sup>, or in low-density 2D electron systems at high enough temperatures<sup>30</sup>.

In graphene, the solution of the kinetic equation is simplified by the kinematic peculiarity of electron-electron scattering leading to a formal divergence of the collision integral known as the “collinear scattering singularity”<sup>18,19,24,27,31–33</sup>. This is another consequence of the Dirac-like spectrum: the energy and momentum conservation laws are identical for quasiparticles moving in the same direction. Although the divergence is regularized by dynamical screening<sup>24,27,33</sup>, the remaining separation in the values of the scattering rates allows for a nonperturbative solution to the kinetic equation facilitating the transition from the microscopic theory to the hydrodynamic description<sup>28</sup>.

The two-fluid hydrodynamic approach can be extended to double-layer systems<sup>31</sup> used in Coulomb drag measurements<sup>34–38</sup>. The resulting theory yields a quantitative description of giant magnetodrag in graphene at charge neutrality<sup>38</sup>. Practical calculations within this approach involve solving the hydrodynamic equations taking into account boundary conditions at the sample edges uncovering the key role of quasiparticle recombination processes in transport measurements in mesoscopic-sized samples. Qualitatively, one can interpret the results of this theory in terms of a semiclassical two-band model<sup>39</sup>. Treating this model phenomenologically, one can extend the hydrodynamic theory to further 2D two-component material near charge neutrality. In particular, the theory suggests an explanation for the phenomenon of linear magnetoresistance in nearly compensated materials in classically strong magnetic fields<sup>40</sup>.

The interest in hydrodynamic behavior of charge carriers in graphene is fueled by a promise for potential applications<sup>41,42</sup>, as well as the exciting prospect of observing phenomena otherwise belonging to the realms of high-energy and plasma physics in a condensed matter laboratory<sup>43</sup>. Recent progress in experimental techniques<sup>44–49</sup> brings the studies of nonlinear phenomena<sup>28</sup> within reach. Nonlocal transport phenomena are already a subject of intensive research<sup>12,50–52</sup>. At the same time, the connection between the nearly relativistic hydrodynamics in graphene<sup>26</sup> and the holography approach to quantum field theory<sup>53,54</sup> represents a promising avenue for theoretical developments.

In this paper, we briefly review the current status of the fast developing field of electron hydrodynamics in

graphene. We begin with the overview of the theory, focusing on the symmetry properties of Dirac quasiparticles in graphene and consequent peculiarities of the derivation of the hydrodynamic equations. Then we discuss several examples of applications of the hydrodynamic approach to experimentally relevant problems including linear magnetoresistance and giant magnetodrag. Finally, we discuss the recent experiments on hydrodynamic flow of graphene. We conclude by discussing the possible extension of the hydrodynamic theory onto further solid state systems with nearly relativistic spectra, e.g. Weyl and Dirac semimetals.

## I. ELECTRONIC TRANSPORT IN GRAPHENE: FROM MICROSCOPIC THEORY TO HYDRODYNAMICS

Traditional hydrodynamics<sup>4</sup> describes the system in terms of the velocity field  $\mathbf{v}$ . The equations describing the velocity field (e.g., the Euler equation in the case of the ideal liquid or the Navier-Stokes equation if dissipation is taken into account) can be either inferred from symmetry arguments or derived from the Boltzmann kinetic equation. Both approaches require one to express the fluxes of conserved quantities (energy, momentum, etc.) in terms of  $\mathbf{v}$ . In particular, the viscous terms appearing in the Navier-Stokes equation can be traced to a particular approximation for the momentum flux (or the stress tensor)  $\Pi_{\alpha\beta}$ . The specific form of  $\Pi_{\alpha\beta}$  depends on whether one discusses a usual, Galilean-invariant or a relativistic, Lorentz-invariant system. As graphene possesses neither symmetry, the precise form of the hydrodynamic equations has to be derived from the microscopic kinetic theory.

### A. Kinetic equation

Microscopically, the electronic system can be described by the Boltzmann kinetic equation

$$\mathcal{L}f = St_{ee}[f] - \tau_{\text{dis}}^{-1}(f - \langle f \rangle_{\varphi}), \quad (1)$$

with the standard Liouvillian form in the left-hand side,

$$\mathcal{L} = \partial_t + \mathbf{v} \cdot \nabla_{\mathbf{r}} + [e\mathbf{E} + e(\mathbf{v} \times \mathbf{B})] \cdot \nabla_{\mathbf{k}}, \quad (2)$$

and the collision integral in the right-hand side. Impurity scattering can be described within the usual  $\tau$ -approximation with  $\tau_{\text{dis}}$  being the disorder mean free time. The collision integral  $St_{ee}[f]$  describes electron-electron interaction. Note that in Eq. (2) we consider only the orbital effect of the magnetic field. The Zeeman splitting is small and plays no role in the context of quasiclassical transport in relatively weak magnetic fields.

The strength of the electron-electron interaction is typically described by the effective interaction constant,  $\alpha_g = e^2/\epsilon v_g$ , where  $\epsilon$  is the effective dielectric constant

of the substrate and  $v_g$  is the quasiparticle velocity in graphene,  $v_g = |\mathbf{v}|$ . Depending on the substrate, the coupling constant may be small<sup>38,55,56</sup>,  $\alpha_g < 1$ . In that case, the solution of the kinetic equation (1) is facilitated by the so-called collinear scattering singularity. Indeed, scattering of quasiparticles with the collinear velocities results in a divergence<sup>18,19,24,27,31–33</sup> in  $St_{ee}[f]$ . The formal divergence is regularized by dynamical screening<sup>24,27,33</sup> leaving generic relaxation rates finite, but large,  $\tau_g^{-1} \propto |\ln \alpha_g| \gg 1$ . At the same time, macroscopic currents related to conserved quantities (i.e. the energy current  $\mathbf{j}_E$  and the electric current  $\mathbf{j}$ ), as well as the so-called imbalance current<sup>17</sup>  $\mathbf{j}_I$ , are relaxed at much longer time scales. This scale separation is the key point allowing for a nonperturbative solution of the kinetic equation (1).

In graphene, the energy current  $\mathbf{j}_E$  is proportional to the momentum and hence cannot be relaxed by electron-electron interaction. Therefore, the steady state cannot be established without some extrinsic mechanism (except for the neutrality point, where in the absence of magnetic field the steady state can be established by Coulomb interaction alone). Therefore, weak disorder scattering has to be taken into account. The relative weakness of potential disorder in the hydrodynamic regime is characterized by the condition

$$\tau_{ee} \ll \tau_{\text{dis}}. \quad (3)$$

Similarly, any other scattering process, such as electron-phonon, quasiparticle recombination, or three-particle processes, should also be characterized by time scales that are much longer than  $\tau_{ee}$ .

Scale separation in  $St_{ee}[f]$  results in the two-step thermalization in graphene. Short-time scattering processes (characterized by  $\tau_g$ ) establish the so-called “unidirectional thermalization”<sup>31</sup>: the collinear scattering singularity implies that the electron-electron interaction is more effective along the same direction. At this point one can solve the kinetic equation within linear response<sup>27</sup>. The resulting non-equilibrium distribution function is proportional to the three macroscopic currents,  $\mathbf{j}$ ,  $\mathbf{j}_E$ , and  $\mathbf{j}_I$ , which can be found from the macroscopic equations obtained by integrating Eq. (1). This approach is reviewed in the next subsection.

At longer time scales, scattering processes characterized by  $\tau_{ee}$  thermalize quasiparticles with different directions of their velocity and hence establish the local equilibrium<sup>28</sup>. Consequently, at longer times the system can exhibit a true hydrodynamic behavior described by nonlinear equations analogous to the classical Navier-Stokes equation. Linearizing these equations one recovers the macroscopic equations of the linear response theory.

## B. Macroscopic linear response theory

Electronic transport in graphene within linear response can be described in terms of the three macroscopic cur-

rents in the system<sup>27</sup>: the energy current  $\mathbf{j}_E$ , the electric current  $\mathbf{j}$ , and the imbalance current (or total quasiparticle flow)  $\mathbf{j}_I$ . While physically inequivalent, the three 2D vectors cannot be linearly independent. It is not surprising, that several two-fluid descriptions of graphene considered either  $\mathbf{j}$  and  $\mathbf{j}_E$ <sup>18,20,26,31</sup>, or  $\mathbf{j}$  and  $\mathbf{j}_I$ <sup>17,38</sup>. In particular, in the so-called Fermi-liquid regime of very high doping all three currents are equivalent. In this simplest case, the theory is reduced to the standard macroscopic electrodynamics (ultimately, Ohm’s law) that can be derived perturbatively<sup>57</sup>.

The theory also simplifies at charge neutrality, where relatively simple equations exhibit all qualitative features of the theory. Consider first an infinite system (meaning that the sample size is much larger than any dynamic length scale in the system). Then the quasiparticle system is essentially uniform and can be described by the following equations (which essentially generalize the Ohm’s law to the case of neutral graphene):

$$\mathbf{E} + \mathcal{R}_H \mathbf{K} \times \mathbf{e}_B = \mathcal{R}_0 \mathbf{j} + \frac{\pi \mathbf{j}}{2e^2 T \tau_{vv} \ln 2}, \quad (4a)$$

$$\mathcal{R}_H \mathbf{j} \times \mathbf{e}_B = \mathcal{R}_0 \frac{e}{2T \ln 2} \mathbf{j}_E, \quad (4b)$$

$$\mathcal{R}_H \mathbf{j} \times \mathbf{e}_B = e \mathcal{R}_0 \mathbf{j}_I + \frac{\pi \mathbf{C}}{2e^2 T \tau_{ss} \ln 2}. \quad (4c)$$

Here  $\mathbf{e}_B$  is the unit vector in the direction of the magnetic field, the coefficients with dimensions of resistivity are

$$\mathcal{R}_0 = \frac{\pi}{2 \ln 2 e^2 T \tau_{\text{dis}}}, \quad \mathcal{R}_H = \frac{\pi \omega_B}{2 \ln 2 e^2 T}, \quad \omega_B = \frac{ev_g^2 B}{2 \ln 2 cT},$$

the vector  $\mathbf{C}$  is a linear combination

$$\mathbf{C} = e \mathbf{j}_E \frac{\gamma_0}{2T \Delta(0) \ln 2} - e \mathbf{j}_I \frac{\mathcal{N}_2(0)}{\Delta(0)},$$

with the numerical coefficients

$$\gamma_0 = \frac{\pi^2}{12 \ln^2 2} \approx 1.7119, \quad \mathcal{N}_2(0) = \frac{9\zeta(3)}{8 \ln^3 2} \approx 4.0607,$$

and

$$\Delta(0) = \gamma_0^2 - \mathcal{N}_2(0) \approx -1.1303,$$

the scattering rates  $\tau_{vv}^{-1}$  and  $\tau_{ss}^{-1}$  describe the mutual scattering in the velocity (electric current) and imbalance channels (in the Fermi liquid limit the rate  $\tau_{vv}^{-1}$  and the vector  $\mathbf{C}$  vanish due to restored Galilean invariance; as a result, electron-electron interaction has no effect on electrical resistivity), and finally the Lorentz term in Eq. (4a) is determined by the vector

$$\mathbf{K} = \mathbf{j} \times \mathbf{e}_B \frac{\kappa \mathcal{R}_H}{\mathcal{R}_0 \Delta(0)},$$

where

$$\kappa = \gamma_0 - 1 + [\gamma_0 - \mathcal{N}_2(0)] \frac{\Delta(0) - \gamma_0 \tau_{\text{dis}} / \tau_{ss}}{\Delta(0) - \mathcal{N}_2(0) \tau_{\text{dis}} / \tau_{ss}} < 0.$$

With the above vector  $\mathbf{K}$ , the direction of the Lorentz term in Eq. (4a) coincides with the direction of  $\mathbf{j}$ . Thus, no classical Hall voltage can be induced at the Dirac point (as expected from symmetry considerations)

$$R_H(\mu = 0) = 0. \quad (5)$$

The equations (4) describe positive magnetoresistance in neutral graphene: the longitudinal magnetoresistance exhibits a quadratic  $B$ -dependence (here both  $\kappa$  and  $\Delta(0)$  are negative, so their ratio is positive)<sup>18,27</sup>

$$R(B; \mu = 0) = R(B = 0; \mu = 0) + \delta R(B; \mu = 0),$$

$$\delta R(B; \mu = 0) = \frac{\mathcal{R}_H^2 \kappa}{\mathcal{R}_0 \Delta(0)} \propto \frac{v_g^4 \tau_{\text{dis}} B^2}{c^2 T^3}. \quad (6)$$

Physically, this result follows from the fact that at charge neutrality electron-electron scattering involves carriers from both bands in graphene. In this sense, the positive magnetoresistance (6) is similar to the well-known classical magnetoresistance in multiband semiconductors.

If the sample is doped away from neutrality, the role of the second band gradually diminishes until the single-band degenerate limit (the Fermi liquid limit) is reached. At this point the classical Hall effect is restored, while the magnetoresistance (4) vanishes. Given the inverse proportionality between the classical Hall coefficient and the carrier density,  $R_H(\mu \gg T) \sim 1/(nec)$ , the Hall coefficient exhibits a maximum at  $\mu \sim T$  in agreement with experiment<sup>58</sup>.

Finally, the equation (4b) becomes meaningless in the absence of disorder scattering, i.e. for  $\mathcal{R}_0 = 0$ . This is a manifestation of the fact that the electron-electron interaction is insufficient to establish the steady state in the system: without extrinsic scattering mechanisms, the energy current (proportional to the total momentum conserved in electron-electron scattering processes) will increase indefinitely under external bias.

### C. Nonlinear hydrodynamic equations for charge carriers in graphene

The linear response theory reviewed in the previous subsection is valid at all time scales greater than  $\tau_g$ . At the same time, in the interaction-dominated regime (3) there is a wide window of parameters where the quasiparticle flows in graphene are truly hydrodynamic.

Indeed, at time scales of order  $\tau_{ee} \gg \tau_g$  the electron-electron scattering processes lead to thermalization of quasiparticles moving in different direction yielding a transition from unidirectional thermalized state to local

equilibrium. The latter is described by the distribution function<sup>23,28</sup>

$$f_{\lambda, \mathbf{k}}^{(0)}(\mathbf{r}) = \{1 + \exp[\beta(\mathbf{r})(\epsilon_{\lambda, \mathbf{k}} - \mu_{\lambda}(\mathbf{r}) - \mathbf{u}(\mathbf{r}) \cdot \mathbf{k})]\}^{-1}, \quad (7)$$

where  $\epsilon_{\lambda, \mathbf{k}} = \lambda v_g k$  denotes the energies of the electronic states with the momentum  $\mathbf{k}$  in the band  $\lambda = \pm 1$ ,  $\mu_{\lambda}(\mathbf{r})$  the local chemical potential, the local temperature is encoded in  $\beta(\mathbf{r}) = 1/T(\mathbf{r})$ , and  $\mathbf{u}(\mathbf{r})$  is the hydrodynamic velocity. The latter should not be confused with the quasiparticle velocity  $\mathbf{v}$  and is defined by its relation to the conserved hydrodynamic current in the system, i.e. the energy current [this relation can be found by substituting the distribution function (7) into the microscopic definition of the energy current; hereafter we use the units with  $v_g = 1$ ]

$$\mathbf{j}_E = \frac{3n_E \mathbf{u}}{2 + u^2}, \quad (8)$$

where  $u = |\mathbf{u}|$ .

The particular form of Eq. (7) reflects the symmetry properties of the two-particle (electron-electron) scattering: conservation of energy, momentum, and the particle number in each band independently. The latter is strictly speaking violated by Auger processes, quasiparticle recombination, and three-particle collisions, but all such processes are assumed to be weak, i.e. characterized by very long scattering times (at least of order  $\tau_{\text{dis}}$ ). Neglecting these processes for the time being, one arrives at the three continuity equations for the hydrodynamic densities

$$\partial_t n + \nabla \cdot \mathbf{j} = 0, \quad (9a)$$

$$\partial_t n_I + \nabla \cdot \mathbf{j}_I = 0, \quad (9b)$$

$$\partial_t n_E + \nabla \cdot \mathbf{j}_E = e \mathbf{E} \cdot \mathbf{j}, \quad (9c)$$

as well as the equation for the energy current

$$\partial_t j_{E, \alpha} + \nabla_{\beta} \Pi_{\beta \alpha}^E - en E_{\alpha} - en(\mathbf{u} \times \mathbf{B})_{\alpha} = -j_{E, \alpha} / \tau_{\text{dis}}. \quad (10)$$

The equation (10) generalizes the usual starting point for derivation of hydrodynamic equations: one has to relate the momentum flux  $\Pi_{\alpha \beta}^E$  to the hydrodynamic velocity  $\mathbf{u}$ . In graphene this can be done with the help of Eq. (7):

$$\Pi_{\alpha \beta}^E = \frac{n_E}{2 + u^2} [\delta_{\alpha \beta} (1 - u^2) + 3u_{\alpha} u_{\beta}] + \delta \Pi_{\alpha \beta}^E. \quad (11)$$

The last term  $\delta \Pi^E$  describes the dissipative effects not included in Eq. (7). The first term is the generalization of the standard stress tensor of an ideal liquid<sup>4</sup> to the case of Dirac fermions. Its unusual form reflects the absence of Galilean and Lorentz symmetries in graphene.

Furthermore, in contrast to the standard hydrodynamics of an electrically neutral fluid<sup>4</sup> the continuity equation for the energy density (9c) contains the ‘‘source term’’

physically corresponding to Joule's heat. This term (naturally absent in the linear response theory) connects the different macroscopic currents reflecting the multiband nature of graphene. In terms of the hydrodynamic velocity, the electric and imbalance currents are given by

$$\mathbf{j} = n\mathbf{u} + \delta\mathbf{j}, \quad (12a)$$

$$\mathbf{j}_I = n_I\mathbf{u} + \delta\mathbf{j}_I, \quad (12b)$$

where again the dissipative corrections  $\delta\mathbf{j}$ ,  $\delta\mathbf{j}_I$  are introduced.

Finally, the electric field in Eqs. (9c) and (10) should include the self-consistent Vlasov field

$$\mathbf{E}_V(\mathbf{r}) = -\nabla_{\mathbf{r}} \int d^2r' V(\mathbf{r} - \mathbf{r}') \delta n(\mathbf{r}'), \quad (13)$$

where  $\delta n(\mathbf{r}) = n(\mathbf{r}) - n_0$  is the fluctuation of the local charge density,  $n_0$  is the background charge density, and  $V(\mathbf{r}) = e^2/r$  is the (3D) Coulomb potential.

Neglecting the dissipative corrections  $\delta\mathbf{j}$ ,  $\delta\mathbf{j}_I$ , and  $\delta\Pi_{\alpha\beta}^E$ , the equations presented in this subsection describe the ideal flow of electronic fluid in graphene<sup>28</sup> generalizing the usual Euler equation<sup>4</sup>. Taking into account dissipative processes one arrives at the generalized Navier-Stokes equation<sup>28</sup>.

The dissipative corrections  $\delta\mathbf{j}$  and  $\delta\mathbf{j}_I$  can be found to leading order in the gradient expansion<sup>28</sup> and have the form

$$\begin{pmatrix} \delta\mathbf{j} \\ \delta\mathbf{j}_I \end{pmatrix} = \mathcal{C}_J^{-1} \boldsymbol{\nu}_J, \quad (14a)$$

where the vector  $\boldsymbol{\nu}_J$  is given by

$$\boldsymbol{\nu}_J = \begin{pmatrix} \frac{n}{3n_E} \nabla n_E - \frac{1}{2} \nabla n - \left[ \frac{2en^2}{3n_E} - \frac{e}{2} \partial_\mu n \right] \mathbf{E} \\ \frac{n_I}{3n_E} \nabla n_E - \frac{1}{2} \nabla n_I - \left[ \frac{2enn_I}{3n_E} - \frac{e}{2} \partial_\mu n_I \right] \mathbf{E} \end{pmatrix}, \quad (14b)$$

and the matrix  $\mathcal{C}_J$  is the reduced collision integral (within the same three-mode approximation as in the previous subsection). Its inverse is given by

$$\mathcal{C}_J^{-1} = \begin{pmatrix} \tau_1 & \tau_2 \\ \tau_3 & \tau_4 \end{pmatrix}, \quad (14c)$$

where  $\tau_j$  are the transport scattering times. The off-diagonal times  $\tau_{2,3}$  change their sign under  $n \rightarrow -n$ . In the non-degenerate regime  $\mu \ll T$  the times  $\tau_j$  are determined by temperature and electron-electron interaction,  $\tau_j = f_j(\mu/T)/(\alpha_g^2 T)$ , where  $f_j(\mu/T)$  is a smooth, dimensionless function. Close to the neutrality point,

$$\tau_2 = \tau_3 = 0, \quad (15a)$$

while

$$\tau_1^{-1} \approx 2.22 \alpha_g^2 T, \quad (15b)$$

and

$$\tau_4^{-1} \approx 0.05 \alpha_g^2 T. \quad (15c)$$

In the degenerate regime,  $\mu \gg T$ , the system behaves similarly to the usual Fermi liquid, where all macroscopic currents are equivalent and electron-electron interaction does not affect transport. Physically, this happens due to the restored Galilean invariance, while technically the interaction-induced transport relaxation rate  $\sim T^4/\mu^3$  (which is the same for all currents) is much smaller than the rate  $\tau_{ee}^{-1} \sim T^2/\mu$  determining the quasiparticle lifetime as well as thermalization.

To leading order in weak deviations from local equilibrium ( $\delta n_E/n_E \ll 1$ ,  $T\delta n_I/n_E \ll 1$ , and  $T\delta n/n_E \ll 1$ ), the correction  $\delta\Pi^E$  takes the canonical form<sup>4</sup>

$$\delta\Pi_{\alpha\beta}^E = -\eta [\nabla_\alpha u_\beta + \nabla_\beta u_\alpha - \delta_{\alpha\beta} \nabla \cdot \mathbf{u}], \quad (16)$$

with  $\eta$  being the viscosity coefficient (from the viewpoint of the hydrodynamic theory this relation is the definition of viscosity; note the absence of the bulk viscosity in this theory). Close to the neutrality point<sup>28</sup>, the viscosity is given by

$$\eta = T(\tau_{\pi,1}n + \tau_{\pi,2}n_I)/4 + 3\tau_{\pi,3}n_E/8, \quad (17)$$

where the scattering times  $\tau_{\pi,i}$  are obtained from the collision integral<sup>28</sup> similarly to the above times  $\tau_i$ , see Eq. (14c). At charge neutrality, the first term in Eq. (17) does not contribute ( $\tau_{\pi,1} = 0$ ), while the remaining time scales  $\tau_{\pi,2(3)} \sim 1/(\alpha_g^2 T)$  are of the same order as Eqs. (15). As a result<sup>21,28</sup>,

$$\eta(\mu = 0) \sim T^2/\alpha_g^2. \quad (18)$$

In the degenerate regime,  $\mu \gg T$ , the usual Fermi-liquid viscosity is recovered<sup>4,28,59</sup>

$$\eta(\mu \gg T) \propto 1/T^2. \quad (19)$$

The expressions for the dissipative correction in terms of the hydrodynamic velocity and densities allow one to close the set of the hydrodynamic equations. In particular, the generalized Navier-Stokes equation can be written in the canonical form<sup>21,28</sup>

$$W\partial_t \mathbf{u} + W(\mathbf{u} \cdot \nabla) \mathbf{u} + \nabla P + \mathbf{u} \partial_t P + \mathbf{u}(\delta\mathbf{j} \cdot \mathbf{E}) \quad (20)$$

$$= en[\mathbf{E} - \mathbf{u}(\mathbf{u} \cdot \mathbf{E})] + \eta \nabla^2 \mathbf{u},$$

where the hydrodynamic pressure is

$$P = \frac{(1 - u^2)n_E}{2 + u^2}, \quad (21)$$

and the enthalpy of the system  $W = n_E + P$  is given by

$$W = \frac{2w}{2 + u^2}, \quad w = n_E + P_0 = 3n_E/2, \quad (22)$$

with the latter being the linear enthalpy of graphene. For small velocities, the pressure assumes the standard value for a scale invariant gas,  $P_0 = n_E/2$ . For large velocities  $u \lesssim 1$  it vanishes as  $\sim (1 - u^2)$ .

The generalized Navier-Stokes equation (20), the continuity equations (9), the Vlasov self-consistency (13), and the expressions for the dissipative corrections (16) and (14) constitute the complete hydrodynamic description of charge carriers in graphene.

## II. SIGNATURES OF HYDRODYNAMIC BEHAVIOR IN GRAPHENE

### A. Longitudinal conductivity in monolayer graphene

As discussed above, a highly nontrivial feature of graphene is that inelastic electron-electron collisions may limit the conductivity at the Dirac point without any disorder or phonon scattering<sup>17,18,20,24,32</sup>. This peculiarity of graphene – which should be contrasted to conventional systems where interactions do not lead (in the absence of Umklapp scattering) to finite resistivity – is a consequence of the particle-hole symmetry and decoupling between velocity and momentum. As a result, although the total momentum of interacting particles is conserved during inelastic collisions, the total current may relax. The collision-limited conductivity of undoped graphene is found<sup>19,24,28,32</sup> to be inversely proportional to  $\alpha_g^2$

$$\sigma(\mu = 0) \approx \frac{e^2}{h} \frac{0.76}{\alpha_g^2}, \quad (23)$$

and depends on temperature only through the renormalization of  $\alpha_g$ <sup>56</sup>. Potential disorder introduces relaxation of the quasiparticle velocity affecting the transport scattering rate due to electron-electron scattering. Moreover, in the presence of disorder the density of states at the Dirac point becomes nonzero. As a result, the conductivity (23) is modified to

$$\sigma(\mu = 0) \sim \frac{e^2}{h} \frac{T + \tau_{\text{dis}}^{-1}}{\alpha_g^2 T + \tau_{\text{dis}}^{-1}}, \quad (24)$$

Away from the Dirac point, the dc conductivity of graphene diverges in the absence of extrinsic scattering, since the momentum and velocity modes are no longer orthogonal to each other. Still, however, inelastic electron-electron collisions that establish the hydrodynamic regime play an important role for transport in clean graphene samples, in particular, in suspended graphene.

Transport properties of suspended graphene<sup>60</sup> were explored in Ref. 61, with a particular focus on the case of zero chemical potential. The interplay of electron-electron collisions with the disorder-induced scattering and interaction with flexural (out-of-plane deformation)

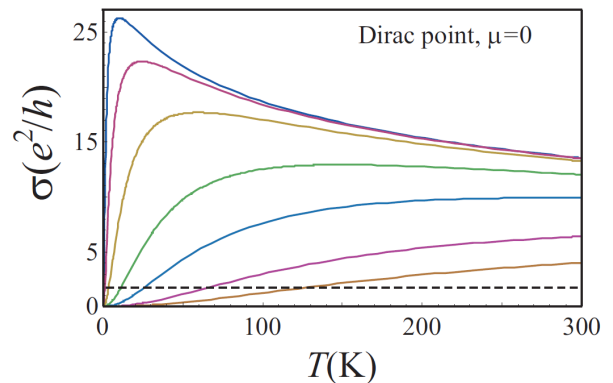


FIG. 1: Temperature dependence of conductivity of suspended graphene at the Dirac point; impurity concentration  $n_i$  grows from top to bottom. Adapted from Ref. 61.

phonons was analyzed. The temperature dependence of the conductivity, Fig. 1, is governed by the electron-impurity (lowest  $T$ ), electron-electron (intermediate  $T$ ), and electron-phonon (highest  $T$ ) scattering. The hydrodynamic description is thus valid in a rather broad range of intermediate temperatures.

### B. Thermal transport in graphene

In a recent paper, Crossno and co-workers<sup>13</sup> have studied the electric and thermal transport in high-quality monolayer graphene samples encapsulated in hexagonal boron nitride. They have evaluated the Lorentz number characterizing the ratio of the thermal conductivity to the electric one. In conventional transport regime, the Lorentz number takes a universal value depending on fundamental constants only. This reflects the fact that the relaxation of charge current and of the thermal current is provided by the same scattering processes. Indeed, Crossno et al. do find this universal value in the most part of the parameter plane spanned by the temperature and the charge carrier density. However, in a relatively narrow range of concentrations around zero (i.e., for the chemical potential being near the Dirac point of particle-hole symmetry) and at intermediate temperatures between 40 and 100 K, the Lorentz number is found to be much larger than the universal value, with the enhancement factor reaching 22. This remarkable observation is a clear manifestation of the hydrodynamic behavior of charge carriers in graphene, namely, of formation of the electron-hole “Dirac fluid”.

An intuitive explanation of the strong enhancement of Lorentz number in the Dirac fluid regime is as follows. When an electric field is applied, electrons and holes move in opposite directions, and the friction between them (mediated by electron-electron interaction) leads to a finite electric resistivity, see Sec. II A. On the other hand, when a temperature gradient is applied, the electrons and holes move in the same direction, implying

no friction and thus infinite thermal conductivity. An accurate theoretical analysis<sup>17,20,21,62</sup> confirms this conclusion.

The fact that the hydrodynamic behavior emerges only in an intermediate temperature range (between 40 and 100 K in the experiment of Ref. 13) is in full agreement with the discussion in the introductory part of the paper. At low temperatures the transport is dominated by impurity scattering, while at high temperatures the phonon scattering becomes the main scattering mechanism.

Another signature of the hydrodynamic behavior in graphene is the substantial enhancement of a related physical quantity, namely the thermoelectric power<sup>26,63</sup> in high-mobility graphene devices. In contrast to the earlier experiments using graphene on silicon oxide<sup>64</sup>, the new measurements showed that at relatively high temperatures the thermoelectric power significantly exceeds the standard Mott relation<sup>65</sup> approaching the ideal hydrodynamic limit<sup>17,19,20,66</sup>, where (in the absence of disorder) the thermopower equals the thermodynamic entropy per carrier charge. This limit, however, was not reached in the experiment<sup>63</sup>, presumably due to inelastic scattering of charge carriers off the optical phonons which appears to be non-negligible even at temperatures much lower than the phonon frequency. The latter effect demonstrates the upper limit of the temperature window for the hydrodynamic behavior.

Finally, one might expect a similar enhancement of the thermal transport in graphene subjected to an external magnetic field. In the earlier experiments<sup>64,67,68</sup>, the Nernst signal in doped graphene appeared to be in agreement with the generalized Mott relation<sup>69,70</sup> and exhibited strong oscillations<sup>71</sup>. However, at charge neutrality the measurements<sup>64,68</sup> show a large enhancement of the Nernst signal strongly deviating from the Mott relation. The thermoelectric power in magnetic field exhibited similar behavior. While the observed effects may be attributed to either the peculiarities of the zeroth Landau level in graphene<sup>72</sup> or the sample shape dependency of the two-terminal transport measurements near the neutrality point<sup>73</sup>, it would be extremely interesting to study the effect of the magnetic field on the hydrodynamic thermal transport in graphene.

### C. Viscosity and nonlocal transport

Currently, manifestations of viscosity in transport properties of graphene in the hydrodynamic regime attract a great deal of attention. In a recent experiment, Bandurin et al.<sup>12</sup> have measured a negative four-terminal resistance of graphene samples. Specifically, they observed a negative voltage drop in the vicinity of current-injection contacts in an intermediate temperature range (roughly between 100 and 200 K). This remarkable observation provides an unambiguous evidence in favor of “whirlpool” current patterns (vorticity) in graphene as expected for a viscous fluid<sup>51,52,74</sup>.

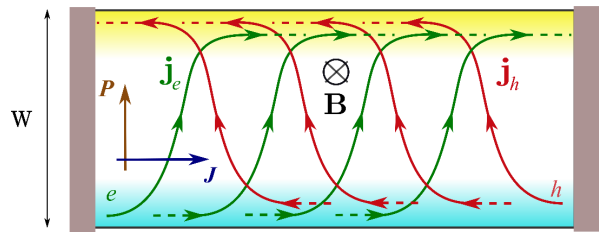


FIG. 2: Electron (green) and hole (red) currents in a finite graphene sample. The quasiparticle flow (denoted by  $P$ ) results in excess quasiparticle density near the sample edges, where recombination processes due to electron-phonon interaction lead to linear magnetoresistance. Adapted from Ref. 39.

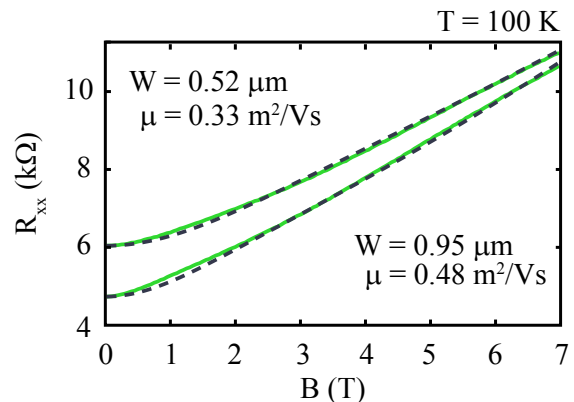


FIG. 3: Magnetoresistance of bilayer graphene measured in two samples<sup>40</sup> with different widths and mobilities at the charge neutrality point and  $T = 100\text{K}$ . Solid (green) lines: experimental data; Dashed (blue) lines: theoretical fit using the semiclassical description of Ref. 39. Adapted from Ref. 40.

In a further recent work, Moll et al.<sup>10</sup> have observed an evidence of the viscous transport predicted in<sup>1</sup> by measuring the resistance of restricted channels of the layered (i.e., essentially two-dimensional) material, PdCoO<sub>2</sub>. This material is known for its purity<sup>75</sup> as evidenced by the extremely small in-plane resistivity and the large mean-free path. Moreover, the ratio of the mean free paths inferred from the analysis of the de Haas-van Alphen effect (a measure of a wide range of scattering processes) and from the resistivity (a measure of momentum relaxation) is about an order of magnitude smaller than that in ordinary metals, indicating that PdCoO<sub>2</sub> is a good candidate for a study of hydrodynamic effects.

### D. Linear magnetoresistance

The hydrodynamic approach to the magnetotransport in infinite graphene samples predicts a positive parabolic magnetoresistance, Eq. (6). However, many magnetotransport experiments in multilayer graphenes exhibit linear magnetoresistance in sufficiently strong magnetic

fields<sup>76–78</sup>. In Refs. 27,39,40,79 it was demonstrated that boundary effects may lead to a non-saturating classical linear magnetoresistance at the charge neutrality point when the sample width is comparable with the electron-hole recombination length  $\ell_0$ .

The mechanism of this boundary effect in the magnetoresistance in a two-component fluid is illustrated in Fig. 2 for an electron-hole symmetric system at charge neutrality, where the Hall effect for electrons is compensated by that for holes. The distribution of electron and hole currents,  $\mathbf{j}_{e,h}$ , differs substantially in the bulk of the sample and near the edges.

The main contribution to the magnetoresistance originates in the narrow edge regions with the width of the order of the recombination length  $\ell_R$ , where both the electron and hole currents are directed essentially along the edge. The edge contribution to the overall resistance at charge neutrality is proportional to  $L/\ell_R$ , where  $L$  is the sample length. With increasing magnetic field, the recombination length gets shorter because of multiple cyclotron returns of electron and holes to each other:  $\ell_R \propto 1/|B|$ . The total sheet resistance  $R_{\square}$  of the sample with the width  $W \gg \ell_R$  can be estimated by treating the edge and the bulk as parallel resistors:  $R_{\square}^{-1} = (R_{\text{bulk}}^{-1} + R_{\text{edge}}^{-1})L/W$ . For sufficiently strong magnetic field  $B$ , the magnetoresistance is then linear in  $B$ :

$$R_{\square} = \frac{1}{e\rho} \frac{W}{\ell_0} |B|, \quad (25)$$

where  $\rho$  is the total quasiparticle density. Away from the charge neutrality, a finite Hall effect leads to a saturation of the linear magnetoresistance. This qualitative derivation<sup>39</sup> is in agreement with the rigorous calculation for graphene<sup>27,79</sup> based on the three-mode hydrodynamic model. This mechanism of linear magnetoresistance was measured in recent experiments on bilayer graphene<sup>40</sup>, see Fig. 3.

### E. Coulomb drag in graphene

Hydrodynamic ideas can also be applied to double-layer systems<sup>34,38,80,81</sup>. Consider a sample consisting of two graphene sheets (or layers) separated by an insulator, that is thick enough, so that the two layers are electrically isolated (i.e., there is essentially no electron tunneling between them), but at the same time not too thick, so that the electric field created by electrons in one layer penetrates into the other. In this case, the inter-layer Coulomb interaction leads to an observable effect known as the Coulomb drag<sup>34</sup>: if an electric current,  $I_1$ , is passed through one of the layers, then a current – or a voltage,  $V_2$ , in the case of an open circuit – will be generated in the other layer. The measured drag coefficient (the ratio of the induced voltage to the driving current,  $R_D = -V_2/I_1$ ) is extremely sensitive to the microscopic structure of the electronic system in the two layers, mak-

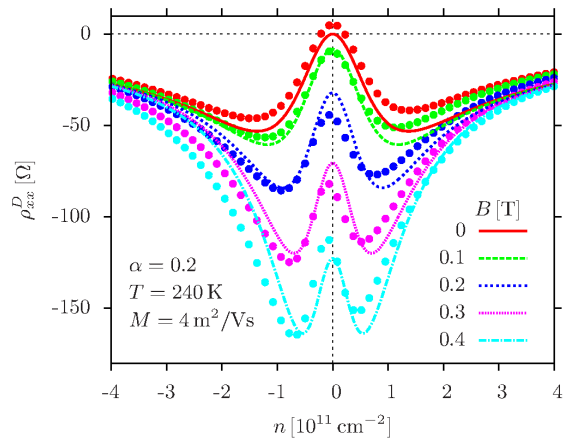


FIG. 4: Giant magnetodrag in graphene. Solid symbols represent the experimental data measured at  $T = 240\text{K}$ . The curves represent the results of theoretical calculations. Both graphene sheets are kept at the same carrier density. Adapted from Ref. 38.

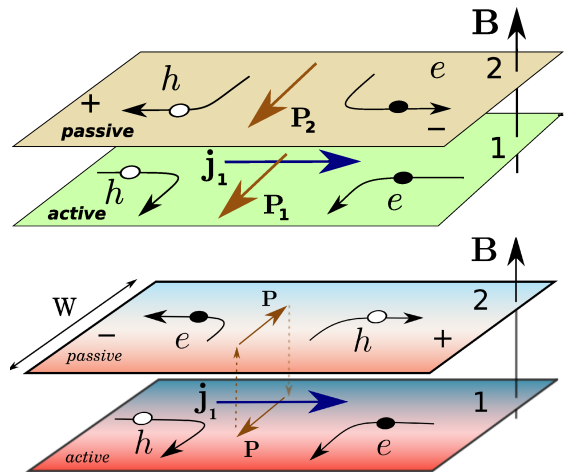


FIG. 5: Qualitative mechanism of magnetodrag in graphene. Top panel: infinite sample, where the lateral quasiparticle flow (denoted by  $\mathbf{P}_i$ ) is transferred between the layers by the Coulomb interaction. Bottom panel: finite-size sample, where the total quasiparticle flow  $\mathbf{P}_1 + \mathbf{P}_2$  in the sample vanishes due to hard wall boundary conditions; this leads to the quasiparticle flows in the two layers having opposite directions,  $\mathbf{P}_1 = -\mathbf{P}_2$ , which leads to negative magnetodrag. Adapted from Ref. 38.

ing it an important tool for experimental studies of many body systems.

The main physical properties distinguishing graphene from conventional conductors – the absence of Galilean invariance, collinear scattering singularity, precise electron-hole symmetry at charge neutrality, unidirectional thermalization, and most importantly, the two-band carrier system – have their direct manifestation in Coulomb drag. In ultra-clean graphene close to charge neutrality, the hydrodynamic description yields



non-trivial, temperature-independent drag resistivity

$$\rho_D \sim \frac{\alpha_g^2}{e^2} \frac{\mu_1 \mu_2}{\mu_1^2 + \mu_2^2}, \quad (26)$$

which remains finite if the chemical potentials of the two layers,  $\mu_1$  and  $\mu_2$ , approach zero simultaneously. However, this result does not survive if even infinitesimal disorder is present in the system, in which case the leading-order contribution to drag vanishes due to the electron-hole symmetry.

The inequivalence of the electric current and macroscopic quasiparticle flow in graphene leads to the effect of giant magnetodrag<sup>38</sup>, see Fig. 4. The effect can be traced back to the fact that the Lorentz force in the electron and hole bands has the opposite sign, which is also the reason for the anomalously large Nernst effect<sup>26,64,67,68</sup> in monolayer graphene and vanishing Hall effect at charge neutrality. Magnetodrag can be qualitatively understood by considering the two-band transport similar to that discussed in Sec. IID above, see Fig. 5. The driving current in a drag experiment corresponds to the counter-propagating flow of electrons and holes, which precisely at the neutrality point is characterized by zero total momentum. This is the physical reason for vanishing drag in the presence of electron-hole symmetry. However, if a weak magnetic field is applied, electrons and holes are deflected by the Lorentz force yielding the neutral quasiparticle flow lateral to the driving current. Now this flow does carry a nonzero momentum which can be transferred to the second layer by the interlayer interaction. There, the Lorentz forces acting on the two types of carriers will drive the charge flow parallel to the driving current and hence yield nonzero magnetodrag. The sign of the effect depends on the geometry of the system.

### F. Nonlinear hydrodynamic phenomena

Nonlinear phenomena (along with the viscous effects discussed below) are the hallmark of the hydrodynamic flow. However, nonlinear effects do not often feature in condensed matter laboratory experiments, where the vast majority of transport measurements are performed within linear response. A notable exception is the experiment of Ref. 5, where signatures of the Gurzhi effect were observed in the nonlinear current-voltage characteristic.

Theoretically, a representative example of nonlinear physics in graphene – relaxation of a hot spot – was discussed in Ref. 28, see Figs. 6 and 7. A hot spot is a nonequilibrium state characterized by a locally elevated quasiparticle energy density. The hot spot can be created using a local probe<sup>44</sup> or a focused laser beam<sup>45</sup>. The experiments of Refs. 44,45 were devoted to the study of plasmon propagation in graphene. In these experiments the samples were continuously illuminated by the external field. In contrast, one can use a single pulse to create nonequilibrium energy density profile and follow the subsequent time evolution. As expected<sup>44,45</sup>, the hot spot

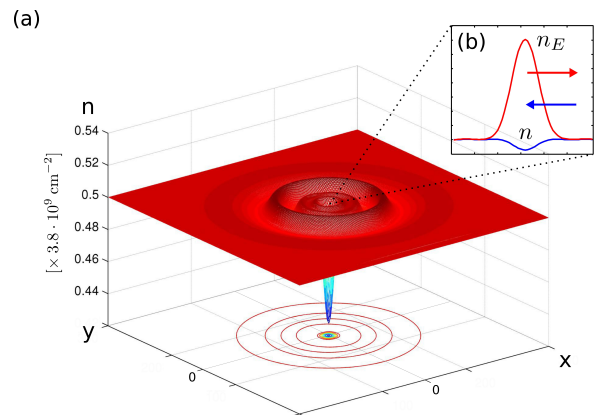


FIG. 6: Hot spot in graphene. Inset: the soliton-like composite object at the origin. The blue curve shows the dip in the charge density, while the red curve shows the excess energy density. The red arrow indicates the pressure force compensated by the self-consistent electric field (shown by the blue arrow). Adapted from Ref 28.

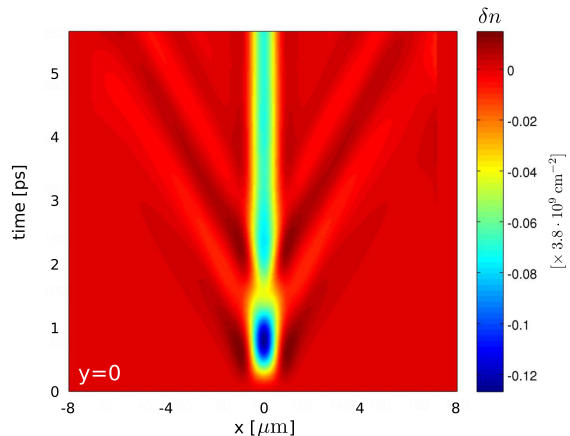


FIG. 7: Hot spot relaxation. The color-map plot shows the time evolution of the charge density as a function of  $x$  along the line  $y = 0$  for short enough time scales. Adapted from Ref. 28.

immediately emits plasmonic waves. However, the nonlinear theory of Sec. IC yields an additional, rather surprising result: a nonzero excess energy density remains at the hot spot accompanied by a nonzero excess charge density.

In graphene, the hydrodynamic energy flow is coupled to the charge flow by means of Vlasov self-consistency (13). At charge neutrality, the two flows may decouple and the hydrodynamic equation (20) admits solutions in the form of energy waves<sup>28,82</sup>. In the absence of dissipation and disorder, the energy wave is acoustic, similar to the “cosmic sound” (i.e. the long-wavelength oscillations in interacting relativistic models)<sup>43</sup>. In a charged system, the self-consistent electric field ensures that the energy waves are accompanied by fluctuations of the charge

density. Physically, the excess energy density leads to the appearance of the pressure force,  $\nabla_\alpha \Pi_{\alpha\beta}^E$ , which in turn initiates the hydrodynamic flow. The corresponding electric current carries charge away from the hot spot leading to a depletion of the charge density. The appearing nonequilibrium profile creates the self-consistent electric field. Remarkably, in the absence of dissipation the generated electric force compensates the above pressure force. As a result, one finds a stable, soliton-like solution with a composite – energy and charge – density profile at the hot spot, see the inset in Fig. 6 (here the initial perturbation of the energy density was chosen to have a form of a Gaussian with the peak height nearly double the unperturbed value,  $n_E = 1.8n_E^{(0)}$  leading to the micrometer size of the soliton). Dissipation leads to decay of the quasi-stable soliton, but this decay occurs at time scales that are long compared to the initial emission of the plasmon waves, see Fig. 7. The plasmon waves themselves are damped by viscous effects.

### III. FINAL REMARKS

Hydrodynamic flow of electrons in solids should be observable not only in graphene, but in any material that is clean enough to satisfy the condition (3). In particular, modern semiconductor technology allows to fabricate ultrahigh-mobility heterostructures<sup>6–8</sup>, which should make it possible<sup>9</sup> to observe hydrodynamic behavior in conventional conductors<sup>30,83,84</sup> for the first time since the original observation of the Gurzhi effect<sup>5</sup>. Very recently, it was suggested that a viscous hydrodynamic flow in electronic systems might exhibit enhanced, higher-than-ballistic conduction<sup>14,85</sup>.

At the same time, hydrodynamic behavior might be observable in a wide range of novel materials including the 2D metal palladium cobaltate<sup>10</sup>, topological insulators<sup>86</sup> (where the conducting surface states may exhibit hydrodynamic behavior), and Weyl semimetals. The latter systems have attracted considerable attention since they exhibit a solid state realization of the Adler-Bell-Jackiw chiral anomaly<sup>87–90</sup>. One of the hallmark manifestations of the anomaly in Weyl systems is the recently observed<sup>90</sup> negative magnetoresistance<sup>89,91–93</sup>. It would be very interesting to observe relativistic Weyl hydrodynamics<sup>93</sup> in these systems.

While the findings reviewed in this paper are highly encouraging, we are only at the beginning of a challenging way towards a better control and understanding of electron fluid mechanics. A further improvement of sample quality is desirable to obtain broader hydrodynamic regimes. It remains to be explored what are possible applications of the emerging “hydrodynamic electronics”.

### Acknowledgments

We would like to thank P.S. Alekseev, U. Briskot, A.P. Dmitriev, L. Fritz, A.K. Geim, R.V. Gorbachev, R.J. Haug, Y.L. Ivanov, V.Y. Kachorovskii, M.I. Katsnelson, A.A. Kozikov, A. Levchenko, J. Link, M. Müller, K.S. Novoselov, P.P. Orth, P.M. Ostrovsky, L.A. Ponomarenko, S. Sachdev, M. Schütt, D.E. Sheehy, A.V. Shytov, D. Smirnov, M. Titov, T. Tudorovskiy, G.Y. Vasileva, Y.B. Vasilyev, and the late A.K. Savchenko for collaboration on the problems reviewed in this paper. This work was supported by the Deutsche Forschungsgemeinschaft via the Priority Program 1459 “Graphene” (I.V.G and A.D.M).

- 
- <sup>1</sup> R. N. Gurzhi, Zh. Eksp. Teor. Fiz. **44**, 771 (1963), [Sov. Phys. JETP **17**, 521 (1963)].
- <sup>2</sup> R. N. Gurzhi, Usp. Fiz. Nauk **94**, 689 (1968), [Sov. Phys. Usp. **11**, 255 (1968)].
- <sup>3</sup> J. L. M. Poiseuille, C. R. Acad. Sci. **11**, 961 (1840).
- <sup>4</sup> L. D. Landau and E. M. Lifshitz, *Fluid Mechanics* (Elsevier Science, 1988).
- <sup>5</sup> M. J. M. de Jong and L. W. Molenkamp, Phys. Rev. B **51**, 13389 (1995).
- <sup>6</sup> L. Bockhorn, P. Barthold, D. Schuh, W. Wegscheider, and R. J. Haug, Phys. Rev. B **83**, 113301 (2011).
- <sup>7</sup> R. G. Mani, A. Krüsa, and W. Wegscheider, Scientific Reports **3**, 2747 (2013).
- <sup>8</sup> Q. Shi, P. D. Martin, Q. A. Ebner, M. A. Zudov, L. N. Pfeiffer, and K. W. West, Phys. Rev. B **89**, 201301 (2014).
- <sup>9</sup> P. S. Alekseev, Phys. Rev. Lett. **117**, 166601 (2016).
- <sup>10</sup> P. J. W. Moll, P. Kushwaha, N. Nandi, B. Schmidt, and A. P. Mackenzie, Science **351**, 1061 (2016).
- <sup>11</sup> K. S. Novoselov, A. K. Geim, S. V. Morozov, D. Jiang, Y. Zhang, S. V. Dubonos, I. V. Grigorieva, and F. A. A., Science **306**, 666 (2004).
- <sup>12</sup> D. A. Bandurin, I. Torre, R. Krishna Kumar, M. Ben Shalom, A. Tomadin, A. Principi, G. H. Auton, E. Khestanova, K. S. Novoselov, I. V. Grigorieva, et al., Science **351**, 1055 (2016).
- <sup>13</sup> J. Crossno, J. K. Shi, K. Wang, X. Liu, A. Harzheim, A. Lucas, S. Sachdev, P. Kim, T. Taniguchi, K. Watanabe, et al., Science **351**, 1058 (2016).
- <sup>14</sup> R. Krishna Kumar, D. A. Bandurin, F. M. D. Pellegrino, Y. Cao, A. Principi, H. Guo, G. H. Auton, M. B. Shalom, L. A. Ponomarenko, G. Falkovich, et al., arXiv:1703.06672.
- <sup>15</sup> L. A. Ponomarenko, A. K. Geim, A. A. Zhukov, R. Jalil, S. V. Morozov, K. S. Novoselov, I. V. Grigorieva, E. H. Hill, V. V. Cheianov, V. I. Falko, et al., Nature Phys. **7**, 958 (2011).
- <sup>16</sup> R. Decker, Y. Wang, V. W. Brar, W. Regan, H.-Z. Tsai, Q. Wu, W. Gannett, A. Zettl, and M. F. Crommie, Nano Letters **11**, 2291 (2011).
- <sup>17</sup> M. S. Foster and I. L. Aleiner, Phys. Rev. B **79**, 085415 (2009).
- <sup>18</sup> M. Müller and S. Sachdev, Phys. Rev. B **78**, 115419 (2008).
- <sup>19</sup> M. Müller, L. Fritz, and S. Sachdev, Phys. Rev. B **78**, 115406 (2008).
- <sup>20</sup> L. Fritz, J. Schmalian, M. Müller, and S. Sachdev, Phys.

- Rev. B **78**, 085416 (2008).
- <sup>21</sup> M. Müller, J. Schmalian, and L. Fritz, Phys. Rev. Lett. **103**, 025301 (2009).
- <sup>22</sup> A. Tomadin and M. Polini, Phys. Rev. B **88**, 205426 (2013).
- <sup>23</sup> D. Svintsov, V. Vyurkov, V. Ryzhii, and T. Otsuji, Phys. Rev. B **88**, 245444 (2013).
- <sup>24</sup> M. Schütt, P. M. Ostrovsky, I. V. Gornyi, and A. D. Mirlin, Phys. Rev. B **83**, 155441 (2011).
- <sup>25</sup> E. M. Lifshitz and L. P. Pitaevskii, *Physical Kinetics* (Pergamon Press (Oxford), 1981).
- <sup>26</sup> S. A. Hartnoll, P. K. Kovtun, M. Müller, and S. Sachdev, Phys. Rev. B **76**, 144502 (2007).
- <sup>27</sup> B. N. Narozhny, I. V. Gornyi, M. Titov, M. Schütt, and A. D. Mirlin, Phys. Rev. B **91**, 035414 (2015).
- <sup>28</sup> U. Briskot, M. Schütt, I. V. Gornyi, M. Titov, B. N. Narozhny, and A. D. Mirlin, Phys. Rev. B **92**, 115426 (2015).
- <sup>29</sup> A. A. Abrikosov and I. M. Khalatnikov, Uspekhi Fiz. Nauk **66**, 177 (1958), [Sov. Phys. Usp. 1, 68 (1958)].
- <sup>30</sup> A. V. Andreev, S. A. Kivelson, and B. Spivak, Phys. Rev. Lett. **106**, 256804 (2011).
- <sup>31</sup> M. Schütt, P. M. Ostrovsky, M. Titov, I. V. Gornyi, B. N. Narozhny, and A. D. Mirlin, Phys. Rev. Lett. **110**, 026601 (2013).
- <sup>32</sup> A. B. Kashuba, Phys. Rev. B **78**, 085415 (2008).
- <sup>33</sup> A. Tomadin, D. Brida, G. Cerullo, A. C. Ferrari, and M. Polini, Phys. Rev. B **88**, 035430 (2013).
- <sup>34</sup> B. N. Narozhny and A. Levchenko, Rev. Mod. Phys. **88**, 025003 (2016).
- <sup>35</sup> R. V. Gorbachev, A. K. Geim, M. I. Katsnelson, K. S. Novoselov, T. Tudorovskiy, I. V. Grigorieva, A. H. MacDonald, S. V. Morozov, K. Watanabe, T. Taniguchi, et al., Nature Physics **8**, 896 (2012), ISSN 1745-2473.
- <sup>36</sup> S. Kim, I. Jo, J. Nah, Z. Yao, S. K. Banerjee, and E. Tutuc, Phys. Rev. B **83**, 161401(R) (2011).
- <sup>37</sup> S. Kim and E. Tutuc, Solid State Commun. **152**, 1283 (2012).
- <sup>38</sup> M. Titov, R. V. Gorbachev, B. N. Narozhny, T. Tudorovskiy, M. Schütt, P. M. Ostrovsky, I. V. Gornyi, A. D. Mirlin, M. I. Katsnelson, K. S. Novoselov, et al., Phys. Rev. Lett. **111**, 166601 (2013).
- <sup>39</sup> P. S. Alekseev, A. P. Dmitriev, I. V. Gornyi, V. Y. Kachorovskii, B. N. Narozhny, M. Schütt, and M. Titov, Phys. Rev. Lett. **114**, 156601 (2015).
- <sup>40</sup> G. Y. Vasileva, D. Smirnov, Y. L. Ivanov, Y. B. Vasilyev, P. S. Alekseev, A. P. Dmitriev, I. V. Gornyi, V. Y. Kachorovskii, M. Titov, B. N. Narozhny, et al., Phys. Rev. B **93**, 195430 (2016).
- <sup>41</sup> S. A. Maier, Nature Phys. **8**, 581 (2012).
- <sup>42</sup> A. N. Grigorenko, M. Polini, and K. S. Novoselov, Nat. Photon. **6**, 749 (2012).
- <sup>43</sup> T. V. Phan, J. C. W. Song, and L. S. Levitov, arXiv:1306.4972.
- <sup>44</sup> Z. Fei, A. S. Rodin, G. O. Andreev, W. Bao, A. S. McLeod, M. Wagner, L. M. Zhang, Z. Zhao, M. Thiemens, G. Dominguez, et al., Nature **487**, 82 (2012).
- <sup>45</sup> J. Chen, M. Badioli, P. Alonso-Gonzalez, S. Thongrattanasiri, F. Huth, J. Osmond, M. Spasenovic, A. Centeno, A. Pesquera, P. Godignon, et al., Nature **487**, 77 (2012).
- <sup>46</sup> T. Taychatanapat, K. Watanabe, T. Taniguchi, and P. Jarillo-Herrero, Nature Phys. **9**, 225 (2013).
- <sup>47</sup> D. N. Basov, M. M. Fogler, A. Lanzara, F. Wang, and Y. Zhang, Rev. Mod. Phys. **86**, 959 (2014).
- <sup>48</sup> P. Alonso-Gonzalez, A. Y. Nikitin, F. Golmar, A. Centeno, A. Pesquera, S. Velez, J. Chen, G. Navickaite, F. Koppens, A. Zurutuza, et al., Science **344**, 1369 (2014).
- <sup>49</sup> A. Woessner, M. B. Lundberg, Y. Gao, A. Principi, P. Alonso-Gonzalez, M. Carrega, K. Watanabe, T. Taniguchi, G. Vignale, M. Polini, et al., Nature Materials **14**, 421 (2015).
- <sup>50</sup> D. A. Abanin, S. V. Morozov, L. A. Ponomarenko, R. V. Gorbachev, A. S. Mayorov, M. I. Katsnelson, K. Watanabe, T. Taniguchi, K. S. Novoselov, L. S. Levitov, et al., Science **332**, 328 (2011).
- <sup>51</sup> L. Levitov and G. Falkovich, Nature Phys. **12**, 672 (2016).
- <sup>52</sup> F. M. D. Pellegrino, I. Torre, A. K. Geim, and M. Polini, Phys. Rev. B **94**, 155414 (2016).
- <sup>53</sup> S. Sachdev, in *From Gravity to Thermal Gauge Theories: The AdS/CFT Correspondence*, edited by E. Papantonopoulos (Springer Berlin, 2011), p. 273, ISBN 978-3-642-04864-7.
- <sup>54</sup> S. A. Hartnoll, A. Lucas, and S. Sachdev, arXiv:1612.07324.
- <sup>55</sup> A. A. Kozikov, A. K. Savchenko, B. N. Narozhny, and A. V. Shytov, Phys. Rev. B **82**, 075424 (2010).
- <sup>56</sup> D. E. Sheehy and J. Schmalian, Phys. Rev. Lett. **99**, 226803 (2007).
- <sup>57</sup> B. N. Narozhny, M. Titov, I. V. Gornyi, and P. M. Ostrovsky, Phys. Rev. B **85**, 195421 (2012).
- <sup>58</sup> K. S. Novoselov, A. K. Geim, S. V. Morozov, D. Jiang, M. I. Katsnelson, I. V. Grigorieva, S. V. Dubonos, and A. A. Firsov, Nature **438**, 197 (2005).
- <sup>59</sup> A. Principi, G. Vignale, M. Carrega, and M. Polini, Phys. Rev. B **93**, 125410 (2016).
- <sup>60</sup> K. I. Bolotin, K. J. Sikes, J. Hone, H. L. Stormer, and P. Kim, Phys. Rev. Lett. **101**, 096802 (2008).
- <sup>61</sup> I. V. Gornyi, V. Y. Kachorovskii, and A. D. Mirlin, Phys. Rev. B **86**, 165413 (2012).
- <sup>62</sup> A. Principi and G. Vignale, Phys. Rev. Lett. **115**, 056603 (2015).
- <sup>63</sup> F. Ghahari, H.-Y. Xie, T. Taniguchi, K. Watanabe, M. S. Foster, and P. Kim, Phys. Rev. Lett. **116**, 136802 (2016).
- <sup>64</sup> Y. M. Zuev, W. Chang, and P. Kim, Phys. Rev. Lett. **102**, 096807 (2009).
- <sup>65</sup> M. Cutler and N. F. Mott, Phys. Rev. **181**, 1336 (1969).
- <sup>66</sup> H.-Y. Xie and M. S. Foster, Phys. Rev. B **93**, 195103 (2016).
- <sup>67</sup> P. Wei, W. Bao, Y. Pu, C. N. Lau, and J. Shi, Phys. Rev. Lett. **102**, 166808 (2009).
- <sup>68</sup> J. G. Checkelsky and N. P. Ong, Phys. Rev. B **80**, 081413 (2009).
- <sup>69</sup> M. Jonson and S. M. Girvin, Phys. Rev. B **29**, 1939 (1984).
- <sup>70</sup> S. M. Girvin and M. Jonson, J. Phys. C **15**, L1147 (1982).
- <sup>71</sup> I. A. Luk'yanchuk, A. A. Varlamov, and A. V. Kavokin, Phys. Rev. Lett. **107**, 016601 (2011).
- <sup>72</sup> D. A. Abanin, K. S. Novoselov, U. Zeitler, P. A. Lee, A. K. Geim, and L. S. Levitov, Phys. Rev. Lett. **98**, 196806 (2007).
- <sup>73</sup> J. R. Williams, D. A. Abanin, L. DiCarlo, L. S. Levitov, and C. M. Marcus, Phys. Rev. B **80**, 045408 (2009).
- <sup>74</sup> I. Torre, A. Tomadin, A. K. Geim, and M. Polini, Phys. Rev. B **92**, 165433 (2015).
- <sup>75</sup> C. W. Hicks, A. S. Gibbs, A. P. Mackenzie, H. Takatsu, Y. Maeno, and E. A. Yelland, Phys. Rev. Lett. **109**, 116401 (2012).
- <sup>76</sup> A. L. Friedman, J. L. Tedesco, P. M. Campbell, J. C. Culbertson, E. Aifer, F. K. Perkins, R. L. Myers-Ward, J. K.

- Hite, C. R. Eddy, G. G. Jernigan, et al., *Nano Letters* **10**, 3962 (2010).
- <sup>77</sup> Z.-M. Liao, H.-C. Wu, S. Kumar, G. S. Duesberg, Y.-B. Zhou, G. L. W. Cross, I. V. Shvets, and D.-P. Yu, *Advanced Materials* **24**, 1862 (2012).
- <sup>78</sup> F. Kisslinger, C. Ott, C. Heide, E. Kampert, B. Butz, E. Spiecker, S. Shallcross, and H. B. Weber, *Nature Phys.* **11**, 650 (2015).
- <sup>79</sup> P. S. Alekseev, A. P. Dmitriev, I. V. Gornyi, V. Y. Kachorovskii, B. N. Narozhny, M. Schütt, and M. Titov, *Phys. Rev. B* **95**, 165410 (2017).
- <sup>80</sup> S. S. Apostolov, A. Levchenko, and A. V. Andreev, *Phys. Rev. B* **89**, 121104 (2014).
- <sup>81</sup> W. Chen, A. V. Andreev, and A. Levchenko, *Phys. Rev. B* **91**, 245405 (2015).
- <sup>82</sup> Z. Sun, D. N. Basov, and M. M. Fogler, *Phys. Rev. Lett.* **117**, 076805 (2016).
- <sup>83</sup> M. Hruska and B. Spivak, *Phys. Rev. B* **65**, 033315 (2002).
- <sup>84</sup> A. Levchenko, H.-Y. Xie, and A. V. Andreev, *Phys. Rev. B* **95**, 121301 (2017).
- <sup>85</sup> H. Guo, E. Ilseven, G. Falkovich, and L. S. Levitov, *Proceedings of the National Academy of Sciences* **114**, 3068 (2017).
- <sup>86</sup> A. P. O. Chan, T. Kvorning, S. Ryu, and E. Fradkin, *Phys. Rev. B* **93**, 155122 (2016).
- <sup>87</sup> S. L. Adler, *Phys. Rev.* **177**, 2426 (1969).
- <sup>88</sup> J. S. Bell and R. Jackiw, *Il Nuovo Cimento A* **60**, 47 (1969), ISSN 1826-9869.
- <sup>89</sup> H. Nielsen and M. Ninomiya, *Physics Letters B* **130**, 389 (1983).
- <sup>90</sup> C.-L. Zhang, S.-Y. Xu, I. Belopolski, Z. Yuan, Z. Lin, B. Tong, G. Bian, N. Alidoust, C.-C. Lee, S.-M. Huang, et al., *Nature Comm.* **7**, 10735 (2016).
- <sup>91</sup> D. T. Son and B. Z. Spivak, *Phys. Rev. B* **88**, 104412 (2013).
- <sup>92</sup> B. Z. Spivak and A. V. Andreev, *Phys. Rev. B* **93**, 085107 (2016).
- <sup>93</sup> A. Lucas, R. A. Davison, and S. Sachdev, *Proceedings of the National Academy of Sciences* **113**, 9463 (2016).